

A Hybrid Model for Erythrocyte Membrane: A Single Unit of Protein Network Coupled with Lipid Bilayer

Qiang Zhu,* Carlos Vera,[†] Robert J. Asaro,* Paul Sche,[†] and L. Amy Sung[†]

*Department of Structural Engineering and [†]Department of Bioengineering, University of California, San Diego, La Jolla, California

ABSTRACT To investigate the nanomechanics of the erythrocyte membrane we developed a hybrid model that couples the actin-spectrin network to the lipid bilayer. This model features a Fourier space Brownian dynamics model of the bilayer, a Brownian dynamics model of the actin protofilament, and a modified wormlike-chain model of the spectrin (including a cable-dynamics model to predict the oscillation in tension). This model enables us to predict the nanomechanics of single or multiple units of the protein network, the lipid bilayer, and the effect of their interactions. The present work is focused on the attitude of the actin protofilament at the equilibrium states coupled with the elevations of the lipid bilayer through their primary linkage at the suspension complex in deformations. Two different actin-spectrin junctions are considered at the junctional complex. With a point-attachment junction, large pitch angles and bifurcation of yaw angles are predicted. Thermal fluctuations at bifurcation may lead to mode-switching, which may affect the network and the physiological performance of the membrane. In contrast, with a wrap-around junction, pitch angles remain small, and the occurrence of bifurcation is greatly reduced. These simulations suggest the importance of three-dimensional molecular junctions and the lipid bilayer/protein network coupling on cell membrane mechanics.

INTRODUCTION

Although the mean size of erythrocytes (red blood cells, or RBC) in their natural state is $\sim 8 \mu\text{m}$, they routinely flow in deformed states through capillaries whose minimum lumen measures $5\text{--}7 \mu\text{m}$ (1) or less and thereafter recover their biconcave shape in low stress states. Essential to this remarkable deformability is a composite membrane consisting of a lipid bilayer coupled to an actin/spectrin-based protein network, the membrane skeleton, which imparts flexibility and integrity to the overall structure. The interest in the mechanical properties of the erythrocyte membrane stems from multiple sources. For example, diseases or disorders such as hereditary spherocytosis, ovalocytosis, and elliptocytosis (2,3) have been shown to be associated with structural alterations in the erythrocyte membrane and the resulting changes in mechanical response (2–5). Another reason for the intense interest is that the erythrocyte membrane has been well characterized, so that it has served as a model system for developing a framework for analyzing the mechanical behavior of a broad range of biological membrane structures (5–7). In addition, useful properties of the composite erythrocyte membrane (strength, lightness, deployability, flexible connectivity, etc.) suggest potential synthetic applications in biomimetics.

Unlike the complicated three-dimensional cytoskeletons in other cells, a mature human erythrocyte has only a thin (yet three-dimensional) skeletal protein network beneath the lipid bilayer (Fig. 1). The network is composed of several major proteins: α - and β -spectrins, ankyrin, band 3, protein 4.1, protein 4.2, and actin, as well as some minor proteins such as myosin, tropomyosin, and tropomodulin (E-Tmod).

Structurally, the network is organized into $\sim 33,000$ repeating units. As revealed by transmission electron microscopy (8–10), each basic repeating unit is viewed as a small spoked but edge-free hexagon (Fig. 2) formed by a junctional complex (JC), with six long $\alpha\beta$ spectrin dimers (Sp) radiating from a central short actin protofilament, and up to six suspension complexes (SC) (11). The radius of a spoked basic unit depends on the degree of extension of the six Sp. These repeating units connect with each other through head-to-head association of Sp from two neighboring units (12). It is important to note that not every Sp dimer is connected to a SC; however, most spectrin tetramers are associated with one (or two) SC. Furthermore, there are $\sim 3\%$ pentagons and 8% heptagons in the network, in addition to 85% hexagons (10). The SC functions as the primary connection between the protein network and the lipid bilayer. A SC consists mainly of band 3, ankyrin, and protein 4.2 (13). While band 3 is a major transmembrane protein (with multiple transmembrane domains) and an anion exchanger, protein 4.2 is myristylated (covalently associated with a completely saturated C14 fatty acid, and therefore tightly associated with the lipid bilayer) (14). The secondary site to link the protein network to the lipid bilayer is at JC, where protein 4.1 is associated with glycophorin C, another transmembrane protein with a single transmembrane domain (15,16).

Because the red cell membrane skeleton has a remarkably simple regular geometry compared to other cell types it has therefore motivated dozens of molecularly inspired modeling efforts, including our three-dimensional network model for a single unit (17). Other recent attempts to describe the mechanical response of the erythrocyte membrane include those of Boey et al. (18), Discher et al. (19), and Li et al. (20). These models are well suited for carrying out analysis of entire cell

Submitted August 1, 2006, and accepted for publication March 13, 2007.

Address reprint requests to L. A. Sung, Tel.: 858-534-5250; E-mail: amysung@bioeng.ucsd.edu.

Editor: Kevin D. Costa.

© 2007 by the Biophysical Society

0006-3495/07/07/386/15 \$2.00

doi: 10.1529/biophysj.106.094383

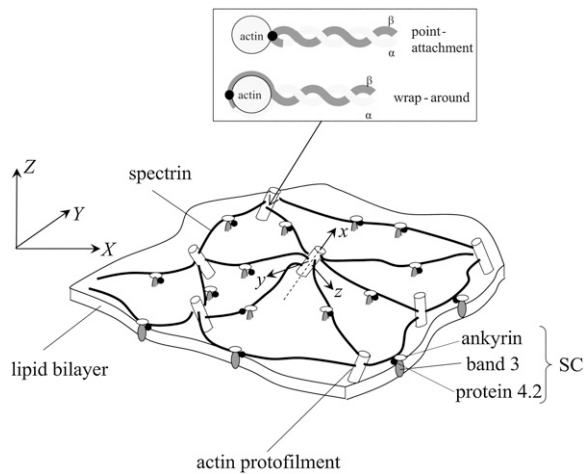


FIGURE 1 Schematic of the erythrocyte membrane showing the connectivity among the major proteins and with the lipid bilayer (modified from (51)). SC, suspension complex. The inset illustrates two possible types of junctions for the Sp/actin attachment, i.e., point-attachment and wrap-around. Small closed circles indicate β -spectrin binding sites on G-actin.

deformation but do not include hydrodynamic effects and are based on an idealized planar picture for the membrane. This makes it difficult to incorporate detailed molecular structure and structural changes that result from, for example, disease or mutation. The model by Hansen et al. (21) was concerned with describing the behavior of planar triangulated meshes of Sp segments modeled as a linear elastic spring. The lipid bilayer was not included, but their modeling did reveal some important effects of network connectivity and topology on the skeleton response and the predicted constitutive properties. The modeling of the lipid bilayer was achieved in Lin and Brown (22), using a Fourier space Brownian dynamics (FSBD) method introduced by Granek (23) to study the mobility of band 3 inside the lipid bilayer. This model did not consider the three-dimensionality and mobility of the protein skeleton and was not intended to probe membrane mechanical properties. It does, however, provide a viable framework for analyzing the dynamics of the lipid bilayer that we use herein.

A complete model for the membrane, i.e., one based on sufficient molecular detail and which would allow detailed correlations between the mechanical response and alterations in the skeletal network, the lipid bilayer, and/or their interconnectivity, would be of considerable value in understanding the dynamic properties of the erythrocyte membrane in normal and diseased states. For example, in disease states such as Southeast Asia ovalocytosis, mutations generate nearly rigid arrays of band 3 cross-linking Sp segments, changing the interconnectivity of the skeleton as well as the skeleton/bilayer connectivity, and leading to dysfunctional mechanical response of the cell (3). It is, accordingly, the intention of this work to develop a molecular-based model of the complete erythrocyte membrane (protein skeleton/lipid bilayer)

that may be used to analyze the deformation behavior of this composite structure.

We propose a hybrid model wherein the three-dimensional dynamic response of a JC and its interaction with the lipid bilayer are accounted for. This model is based on a static model as reported in Vera et al. (17), which features a detailed three-dimensional description of a single JC unit as described by Sung and Vera (11). Numerical results based on this early model revealed that the protofilaments may be more tangent than normal to the lipid bilayer, in agreement with experimental observations made with the micropipette aspiration technique combined with fluorescent polarization microscopy (24,25). Our previous model, however, simplified the lipid bilayer by modeling it as a flat plate connected to the JC via a linear spring, and has not considered important effects such as hydrodynamic drag and thermal fluctuations. In addition, this model depicted the Sp-protofilament junction as a simple attachment point (ball-joint), even though the α - and β -spectrin may wrap around a protofilament (11). The proposed wrap-around junction is based on a three-dimensional model (11) and biochemical interactions between α - and β -spectrin (26–29). The wrap-around junction, adopted herein, features the extension of α - and/or β -spectrin around the protofilament, providing a mechanism to minimize the torque applied to the protofilament during deformation, affecting its roll and possibly yaw motions. It is also understood that the influence of lateral association on forced unfolding of anti-parallel spectrin heterodimers plays an important role in the biomechanics of spectrin and the network (30), and this feature is to be incorporated into our models in the future. Currently, we consider the dynamic response of a fully coupled single unit of JC with the lipid bilayer. Careful attention is paid to describing the dynamic properties of the JC, the junction between Sp and the protofilament, and the interaction between the JC and the lipid bilayer. To achieve this, we model the protofilament as a rigid body and solve its motion by employing the Langevin equation, while the tethering force in Sp is obtained using the wormlike-chain (WLC) paradigm (31). A stochastic term representing thermal effects is incorporated. Domain unfolding in the Sp, as discussed by Rief et al. (32) and Lee and Discher (33) is not included in our present Sp model but can be incorporated as discussed below. The WLC model has been used in most other recent studies (e.g., (18–20)) and thus is chosen here to provide linkage to these studies. The JC is connected to the lipid bilayer through the SCs. In the present study, because this model deals with one single unit of the network, the lateral mobility of these SCs is prohibited, while they are allowed to follow the heaving motion of the bilayer. Two types of Sp-protofilament junction, one corresponding to the point-attachment connection used in the previous study (17) and the other incorporating the torque-minimizing effect of the wrap-around connection are considered and compared with each other. Finally, we model the bilayer via the above mentioned FSBD method. This model is unique in its molecular detail, in its

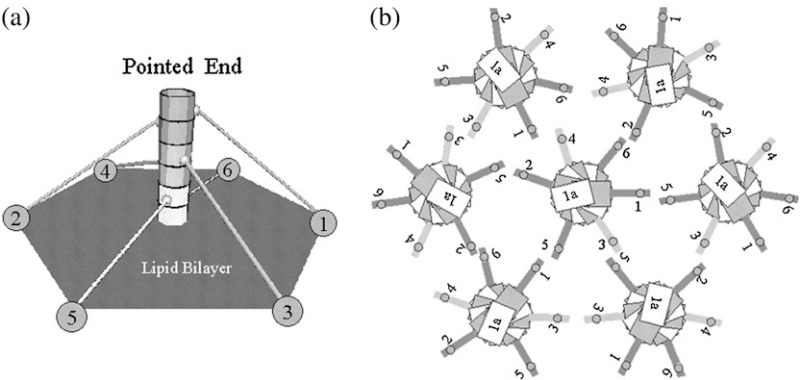


FIGURE 2 (a) Topology of a spoked hexagon (JC) in the erythrocyte membrane skeleton—a three-dimensional view showing a protofilament with six pairs of G actin associated with six Sps. Each Sp may connect to a SC in the lipid bilayer, forming a small hexagon without physical edges. The numbers in the SC indicate the order of G actin pairs, Sp, and SC. The angle between the actin protofilament and the lipid bilayer is not specified and molecules are not to scale. (b) A top view of a large hexagon, formed by six basic hexagonal units surrounding a center unit. The head-to-head interaction of Sp forms a spectrin tetramer between adjacent units. (Both *a* and *b* are from (11).)

accounting for the vital three-dimensionality of the structure, in its inherently time-dependent response, and in its capacity of including fluid effects.

The rest of the article is organized as follows. In the next section we describe the physical model for the JC. The mathematical formulation and numerical algorithms are then detailed for the lipid bilayer and its connectivity to the skeleton. Numerical results, including both quasi-static response of the JC-bilayer structure and effects of thermal fluctuations, are provided. Preliminary calculations of important constitutive parameters such as the shear modulus are made and described. Finally, we summarize the primary findings. As noted, the present work is concerned with the development and implementation of a basic unit of JC/lipid bilayer model. Extensions of the work will include simulations of multiple JC units for the purpose of modeling the effects of topology and connectivity on mechanical response, including mutations of the skeleton/lipid bilayer structure on dynamic and quasi-static response.

MODEL FOR THE JC

Following our first report on the 3-D nanomechanics of an erythrocyte JC in deformation (17), we use Sung and Vera’s 3-D model for the JC (11). An actin protofilament contains 12–13 G-actin arranged in a helical fashion with a dihedral angle (angle between subsequent G actin) of 166.2° and with an axial distance of 5.5 nm. The protofilament is reinforced by two dimeric tropomyosin, one in each of the two grooves, and is capped by an E-Tmod at one end (the pointed end). The positions of β -spectrin binding sites are based on the regularity of G-actin arranged in F-actin, and the predicted occupation of six out of twelve β -spectrin binding sites on the protofilament (11). As shown in Fig. 2 *a*, in a JC, the protofilament functions as a mechanical axis to anchor three (*top*, *middle*, and *bottom*) pairs of Sp. Each Sp pair (i.e., Sp₁/Sp₂, Sp₃/Sp₄, or Sp₅/Sp₆) is arranged in a back-to-back fashion and connects with the protofilament. The Sp pairs spiral down the protofilament in a right-handed manner from the pointed end with a dihedral angle of 55.4° between them.

The detailed coordinates of the β -spectrin binding sites are listed in Table 1.

Our present model depicts a single JC consisting of an actin protofilament (modeled as a rigid circular cylinder with length *b* and radius *a*) and six Sp, coupled to the lipid bilayer. Since the length of the actin protofilament is ~100 times smaller than the persistence length of the actin filament (34), it is reasonable to consider it as a rigid cylinder. The JC is connected to the lipid bilayer through SC. In this model, the actual volume and geometry of the SC are ignored, and thus the Sp is assumed to be connected to the bilayer at point junctions. Note that since we do not allow band 3 motion in the present simulations to move within the lipid bilayer, the Sp are pretensioned as described below.

Coordinate systems

For convenience, the problem is formulated using a Euler-Lagrangian dual-coordinate system (see Fig. 1), including a global space-fixed Euler coordinate system (*X*, *Y*, *Z*) and a local actin-fixed Lagrangian reference frame (*x*, *y*, *z*). The Euler coordinate system is defined so that the undisturbed lipid bilayer lies within the *X*-*Y* plane, and *Z* points toward the JC. The origin of the Lagrangian coordinate system (*x*, *y*, *z*) is at the center of the protofilament, *x* is tangential to the protofilament aligned toward the pointed end capped by E-Tmod, and both *y* and *z* are perpendicular to *x*. In this dual-coordinate system, an arbitrary vector **g** is represented either as (*g_X*, *g_Y*, *g_Z*) in the Euler system, or as (*g_x*, *g_y*, *g_z*) in the Lagrange system. The transformation between these two representations is

TABLE 1 Locations of the Sp-actin attachment sites in the Lagrangian reference frame (*x*, *y*, *z*) (in nm)

	Point-attachment junction	Wrap-around junction
Sp ₁	(12.38, 0, 4.5)	(12.38, 0, 0)
Sp ₂	(9.63, −1.08, −4.37)	(9.63, 0, 0)
Sp ₃	(1.38, 3.70, 2.56)	(1.38, 0, 0)
Sp ₄	(−1.38, −4.21, −1.60)	(−1.38, 0, 0)
Sp ₅	(−9.63, 4.21, −1.60)	(−9.63, 0, 0)
Sp ₆	(−12.38, −3.70, 2.56)	(−12.38, 0, 0)

$$\begin{bmatrix} g_x \\ g_y \\ g_z \end{bmatrix} = \mathbf{C} \cdot \begin{bmatrix} g_X \\ g_Y \\ g_Z \end{bmatrix}, \quad (1)$$

where \mathbf{C} is the orthogonal tensor representing the change of orientation from the global to the local reference frame. Here \mathbf{C} is constructed by using the robust method of Euler parameters. This method is based on Euler's principal rotation theorem (35), which describes an arbitrary reorientation as a single rotation by a principal angle θ about the principal unit vector of \mathbf{C} , i.e., ℓ . Correspondingly, four Euler parameters $\beta_0, \beta_1, \beta_2$, and β_3 are defined as

$$\begin{bmatrix} \beta_0 \\ \beta_1 \\ \beta_2 \\ \beta_3 \end{bmatrix} = \begin{bmatrix} \cos(\theta/2) \\ \ell_x \sin(\theta/2) \\ \ell_y \sin(\theta/2) \\ \ell_z \sin(\theta/2) \end{bmatrix}. \quad (2)$$

We note that the Euler parameters are not independent due to the relation $\beta_0^2 + \beta_1^2 + \beta_2^2 + \beta_3^2 = 1$. The rotation matrix, \mathbf{C} , thus becomes (36)

$$\mathbf{C} = \begin{bmatrix} \beta_0^2 + \beta_1^2 - \beta_2^2 - \beta_3^2 & 2(\beta_1\beta_2 + \beta_0\beta_3) & 2(\beta_1\beta_3 - \beta_0\beta_2) \\ 2(\beta_1\beta_2 - \beta_0\beta_3) & \beta_0^2 - \beta_1^2 + \beta_2^2 - \beta_3^2 & 2(\beta_2\beta_3 + \beta_0\beta_1) \\ 2(\beta_1\beta_3 + \beta_0\beta_2) & 2(\beta_2\beta_3 - \beta_0\beta_1) & \beta_0^2 - \beta_1^2 - \beta_2^2 + \beta_3^2 \end{bmatrix}. \quad (3)$$

Spectrin-actin junction: point-attachment versus wrap-around models

One of the structural characteristics determining the mechanical response of the JC is the exact manner in which a spectrin dimer is connected to the protofilament. In the previous numerical model of a JC (17), this important linkage was simplified as a point-attachment, i.e., an Sp was connected to the protofilament at a single point corresponding to the proposed β -spectrin binding site on the G actin (11) (see the *inset* in Fig. 1). According to this model, the forces applied through Sp will directly affect this binding site. The unfolding of domains would be the primary protective measure, relieving an overly large tensile force on the binding site. Corresponding to this model, the six Sps are pinned at the outer surface of the circular cylinder representing the protofilament.

Compared with the point-attachment junction, the proposed wrap-around junction (11) possesses many advantages in terms of structural stability. As displayed in the *inset* in Fig. 1, the α - and β -spectrins of an Sp are seen to split and wrap around the protofilament and reconnect at the back side. Thus, the tension inside Sp does not impose directly on the binding site; instead, it is distributed around the protofilament. The binding between Sp and protofilament is reversible in the event that dissociation occurs, since Sp is still

wrapped around the protofilament so the configurational entropy increase of a released Sp is small. Furthermore, during deformation the α - and β -spectrin wrapping around the protofilament may stretch so that the roll moment applied to the protofilament is reduced, diminishing the coupling effect between the Sp and the protofilament in the roll mode. Although at this time it is difficult to estimate the exact magnitude of the reduction in coupling, it is reasonable to study an extreme case of complete decoupling in the roll mode. We mathematically simulated this condition by pinning the six Sps along the central axis of the protofilament so that the tension inside an Sp generates no roll moment on the protofilament. The exact locations of these pinning points, as well as the locations of the points where the Sps are attached to the lipid bilayer (corresponding to the locations of the SC), are listed in Tables 1 and 2 (see (11) for additional detail regarding the connection locations). In the following, we address the mathematical formulation and numerical issues in this coupled model.

MATHEMATICAL FORMULATION AND NUMERICAL METHODS

Nonlocal Langevin equation

In the following, we summarize the key steps involved in using the FSBD method (23) to model the dynamics of the lipid bilayer. Additional detail on the FSBD method is found in Lin and Brown (22). Considering a bilayer with uniform tension σ , the layer's elevation, $h(\mathbf{X}, t)$ where $\mathbf{X} = (X, Y)$ is the horizontal position vector, is determined via the nonlocal Langevin equation. This takes the form

$$\frac{\partial h(\mathbf{X}, t)}{\partial t} = \iint d\mathbf{X}' \Lambda(\mathbf{X} - \mathbf{X}') [-\kappa_c \nabla^4 h(\mathbf{X}', t) + \sigma \nabla^2 h(\mathbf{X}', t) + F(\mathbf{X}', t) + \zeta(\mathbf{X}', t)]. \quad (4)$$

TABLE 2 Locations of the SCs in the Euler reference frame (X, Y, Z) (in nm) at natural state with no heave motion in the lipid bilayer

SC number	Location
1	(0, 30, 0)
2	(0, -30, 0)
3	(26, 15, 0)
4	(-26, -15, 0)
5	(26, -15, 0)
6	(-26, 15, 0)

In Eq. 4, $\Lambda(\mathbf{X} - \mathbf{X}') = 1/8\pi\mu_f|\mathbf{X} - \mathbf{X}'|$ is the diagonal component of the Oseen hydrodynamic tensor, μ_f is the dynamic viscosity of the surrounding fluid, and κ_c the bending modulus of the bilayer (so that $-\kappa_c\nabla^4 h$ is a force imposed on the lipid bilayer due to bending). Similarly, due to the existing tension, σ , there is an induced force $\sigma\nabla^2 h$ in the bilayer. $\mathbf{F}(\mathbf{X}', t)$ and $\zeta(\mathbf{X}', t)$ are the interaction force and random thermal fluctuation force, respectively (all forces are measured per unit area of the bilayer). Following Lin and Brown (22), we choose $\kappa_c = 2 \times 10^{-20}$ J and $\mu_f = 0.006$ N/m.

In our present analysis of a single JC unit, the interaction force (acting in the vertical Z direction) is composed of three parts, i.e.,

$$\mathbf{F}(\mathbf{X}, t) = \mathbf{F}^{(c)}(\mathbf{X}, t) + \mathbf{F}^{(p)}(\mathbf{X}, t) + \mathbf{F}^{(s)}(\mathbf{X}, t), \quad (5)$$

where $\mathbf{F}^{(c)}(\mathbf{X}, t)$ represents the force exerted through the tension borne by the Sp, $\mathbf{F}^{(p)}(\mathbf{X}, t)$ is the repulsive force exerted between the actin protofilament and the lipid bilayer, and $\mathbf{F}^{(s)}(\mathbf{X}, t)$ the repulsive force between spectrin and the lipid bilayer; the latter two forces being of a steric type. We note that, since the SCs are taken to be immobile, steric interactions between the Sp segments are negligible, at least for deformations that do not involve large compressive strains. For this reason steric interactions among the Sp are neglected here, but may be explicitly included in much the same way as described above.

Let $\mathbf{X}_i^{(c)}$ ($i = 1, 6$) be the locations of the SCs (Table 1). Then, following Lin and Brown (22), we set

$$\mathbf{F}^{(c)}(\mathbf{X}, t) = \sum_{i=1}^6 \frac{f_{iz}(t)}{\pi(\ell/4)^2} \exp\left(-\left|\frac{\mathbf{X} - \mathbf{X}_i^{(c)}}{c_1/4}\right|^2\right), \quad (6)$$

where $f_{iz}(t)$ is the Z -component of the stretching force inside the i^{th} Sp and c_1 is a localization parameter meaning that the SC force is concentrated in an area of order c_1^2 . By integrating Eq. 6 over the total bilayer area, we find that the total force in the six Sps in the Z direction is indeed $\sum_{i=1}^6 f_{iz}(t)$. To obtain the short-range repulsive interaction force between the actin protofilament and the bilayer, we segment the surface of the protofilament into N_p elements. Each element, with area s_α ($\alpha = 1, \dots, N_p$), is centered at $(\mathbf{X}_\alpha^{(p)}, Z_\alpha^{(p)})$. The repulsive force generated by the actin protofilament on the lipid bilayer is modeled as a short-range force (37). For this we write

$$\mathbf{F}^{(p)}(\mathbf{X}, t) = -\gamma \sum_{\alpha=1}^{N_p} s_\alpha \exp\left(-\frac{Z_\alpha^{(p)} - h(\mathbf{X}, t)}{c_2} - \left|\frac{\mathbf{X} - \mathbf{X}_\alpha^{(p)}}{c_1/4}\right|^2\right), \quad (7)$$

where γ represents the magnitude of interaction and c_2 its steepness, taken to be 0.2 nm. In our simulations, 40 elements were employed.

The repulsive force imposed by the Sp on the bilayer is evaluated in a similar manner. Consider the i^{th} Sp ($i = 1, \dots, 6$); its projection, P_i , on the mean plane of the bilayer ($Z = 0$), is expressed as a straight line, $A_i X + B_i Y + C_i = 0$, bounded by

the projected points of the SC and the Sp-protofilament attachment point. From an arbitrary point on the bilayer, \mathbf{X} , we draw a line that is perpendicular to P_i . The two lines intersect at \mathbf{X}_{Pi} . The Z -coordinate of the Sp right above \mathbf{X}_{Pi} is Z_{Pi} . The repulsive force is then assumed to be zero if \mathbf{X}_{Pi} lies outside of the boundaries of P_i . Otherwise, this force is assumed to be a nonzero repulsive force that decays with the distance between \mathbf{X} and \mathbf{X}_{Pi} , i.e., $|A_i X + B_i Y + C_i|/\sqrt{A_i^2 + B_i^2}$, and increases exponentially with $-(Z_{Pi} - h(\mathbf{X}, t))$. Summing the contribution from all the Sp, we have

$$\mathbf{F}^{(s)}(\mathbf{X}, t) = \eta \sum_{i=1}^6 \exp\left(-\frac{Z_{Pi} - h(\mathbf{X}, t)}{c_2} - \frac{1}{A_i^2 + B_i^2} \left[\frac{A_i X + B_i Y + C_i}{c_1/4}\right]^2\right), \quad (8)$$

where η is a constant characterizing the magnitude of the repulsive interaction.

The random thermal fluctuation force, $\zeta(\mathbf{X}, t)$, is modeled as a Gaussian variable with zero mean, i.e., $\langle \zeta(\mathbf{X}, t) \rangle = 0$, and no temporal correlations, whose variance is

$$\langle \zeta(\mathbf{X}, t) \zeta(\mathbf{X}', t') \rangle = 2k_B T \Lambda^{-1}(\mathbf{X} - \mathbf{X}') \delta(t - t'), \quad (9)$$

where k_B is Boltzmann's constant, T temperature, and δ the Dirac delta-function (38). In all our simulations, $T = 300$ K.

Among the parameters that quantify the interaction forces among the Sp, the bilayer, and the protofilament, some are chosen to be consistent with previous work (22), including $c_1 = 7$ nm and $c_2 = 0.2$ nm. Others (γ and η) are chosen through our numerical tests. We find that when these parameters are not sufficiently large, their respective force expressions will not prevent the protofilament or the Sp from penetrating the bilayer; on the other hand, when their values are too large, extremely small time steps are required for numerical stability. Best results are obtained with $\gamma = 10^{22}$ Nm $^{-4}$ and $\eta = 0.1$ Nm $^{-2}$.

We apply an efficient Fourier spectral algorithm to resolve the nonlocal Langevin equation (23). Assuming that the problem is doubly periodic (with period L) in both X and Y directions, we consider a piece of lipid bilayer whose projection on the X - Y plane is a square with length L in both dimensions. L is chosen to be much larger than the scale of the JC so that disturbances with wavelengths larger than L (representing global deformations) will not have a significant effect on our analysis, which is focused on local responses. Our numerical tests demonstrated that the responses of the JC were not sensitive to the value of L . For any doubly-periodic function $f(\mathbf{X})$, the Fourier transform and reverse Fourier transform are, respectively,

$$\begin{aligned} \tilde{f}(\mathbf{k}) &= \iint_{L \times L} f(\mathbf{X}) \exp(-i\mathbf{k} \cdot \mathbf{X}) d\mathbf{X}, \\ f(\mathbf{X}) &= \frac{1}{L^2} \iint_{L \times L} \tilde{f}(\mathbf{k}) \exp(i\mathbf{k} \cdot \mathbf{X}) d\mathbf{k}. \end{aligned} \quad (10)$$

In Fourier space Eq. 4 becomes

$$\frac{\partial}{\partial t} \tilde{h}(\mathbf{k}, t) = \Lambda(\mathbf{k}) [-(\kappa k^4 + \sigma k^2) \tilde{h}(\mathbf{k}, t) + \tilde{F}(\mathbf{k}, t) + \tilde{\xi}(\mathbf{k}, t)], \quad (11)$$

where $k = |\mathbf{k}|$ and $\Lambda(\mathbf{k}) = 1/4\mu_f k$. Using $N \times N$ Fourier modes we have $\mathbf{k} = (2m\pi/L, 2n\pi/L)$ with $m, n = -N/2, \dots, N/2 - 1$. In Eq. 11 the modes are decoupled and subsequently we numerically integrate it as

$$\tilde{h}(\mathbf{k}, t + \Delta t) = \tilde{h}(\mathbf{k}, t) + \Delta t \Lambda(\mathbf{k}) [-(\kappa k^4 + \sigma k^2) \tilde{h}(\mathbf{k}, t) + \tilde{F}(\mathbf{k}, t) + R(\mathbf{k}, \Delta t)]. \quad (12)$$

When $\mathbf{k} = (0, 0)$, $(-N\pi/L, 0)$, $(0, -N\pi/L)$, or $(-N\pi/L, -N\pi/L)$, the Brownian random term $R(\mathbf{k}, t)$ is a real Gaussian random variable with zero mean and variance $2L^2 k_B T \Lambda(\mathbf{k}) \Delta t$; for other \mathbf{k} -values, $R(\mathbf{k}, t)$ is a complex function whose real and imaginary parts are both Gaussian random variables with zero mean and variance $L^2 k_B T \Lambda(\mathbf{k}) \Delta t$. Once we obtain the updated elevation, $\tilde{h}(\mathbf{k}, t)$, the inverse transform is computed via a FFT so that the computational effort is only proportional to $N^2 \log N^2$.

Dynamics of the actin protofilament

Owing to the small scale of the problem, the inertia of the protofilament is negligible. Its motion is thus determined by the balance among the hydrodynamic viscous drag exerted by the surrounding fluid, the Brownian force/moment, $\mathbf{f}^{(s)}$, $\mathbf{M}^{(s)}$, the force and moment exerted by Sp, $\mathbf{f}^{(s)}$, $\mathbf{M}^{(s)}$, and the repulsive force/moment due to its interaction with the lipid bilayer, $\mathbf{f}^{(b)}$, $\mathbf{M}^{(b)}$. Measured in the Lagrange coordinate system, let the translational velocity of the protofilament be (u_x, u_y, u_z) and its rotational velocity be $(\omega_x, \omega_y, \omega_z)$. Then according to the Langevin equation we have

$$u_i = \frac{f_i^{(s)} + f_i^{(b)} + f_i^{(\xi)}}{D_i}, \quad \omega_i = \frac{M_i^{(s)} + M_i^{(b)} + M_i^{(\xi)}}{D_{Mi}}, \quad (13)$$

$i = x, y, z,$

where D_x is the tangential drag coefficient along the protofilament and $D_y = D_z$ are the normal drag coefficients. D_{Mx} , D_{My} , and D_{Mz} are the drag coefficients associated with rotations around the x , y , z axes, respectively. Using a slender body approximation and assuming that both the tangential drag and the roll drag are caused by skin friction, we find that these drag coefficients are related as $D_{Mx} = a^2 D_x$, $D_{My} = D_{Mz} = b^2 D_y/12$.

The Reynolds number of the flow surrounding the protofilament is usually within the creeping/Stokes regime. Therefore the hydrodynamic effect on the protofilament is modeled by distributing a set of Stokeslets, as demonstrated by Lighthill (39). The normal and tangential drag coefficients per unit length are estimated as, respectively,

$$K_N = \frac{4\pi\mu_f}{\ln(2q/a) + 1/2}, \quad K_T = \frac{2\pi\mu_f}{\ln(2q/a)}, \quad (14)$$

where q is a length scale that measures the correlation length along the length of the protofilament. To evaluate q , we evoke Lamb's theory of two-dimensional creeping flow around a circular cylinder (40) and find that the normal drag coefficient is expressed alternatively as

$$K_N = \frac{4\pi\mu_f}{2 - \ln Re}, \quad (15)$$

where $Re = 2a\rho\sqrt{u_y^2 + u_z^2}/\mu_f$ is the Reynolds number and ρ is the density of the surrounding fluid. The value q is obtained by comparing Eq. 15 with the first of Eq. 14. We then have $D_x = bK_T$, $D_y = D_z = bK_N$.

Following the fluctuation-dissipation theorem, the components of the thermal fluctuation force/moment $f_x^{(\xi)}$, $f_y^{(\xi)}$, $f_z^{(\xi)}$, $M_x^{(\xi)}$, $M_y^{(\xi)}$, and $M_z^{(\xi)}$ are Gaussian random variables with zero mean. The variances for the forces are $2k_B T D_x / \Delta t$, $2k_B T D_y / \Delta t$, and $2k_B T D_z / \Delta t$ and for the moments we have $2k_B T D_{Mx} / \Delta t$, $2k_B T D_{My} / \Delta t$, and $2k_B T D_{Mz} / \Delta t$, respectively. The force caused by interaction of the protofilament with the lipid bilayer, $\mathbf{f}^{(b)}$, is obtained by summing the contributions from the repulsive force acting on each element around its surface. Due to the principle of action and reaction, $f_i^{(b)}$, in turn, is evaluated by integrating its corresponding part in the interaction force over the bilayer with a sign change. This yields

$$f_{z,\alpha}^{(b)}(t) = \gamma \iint_{L \times L} s_\alpha \exp \left(-\frac{Z_\alpha^{(p)} - h(\mathbf{X}, t)}{c_2} - \left| \frac{\mathbf{X} - \mathbf{X}_\alpha^{(p)}}{c_1/4} \right|^2 \right) d\mathbf{X},$$

$\alpha = 1, \dots, N_p.$ (16)

Similarly we obtain the repulsive moment, $\mathbf{M}^{(b)}$, by summing the contributions of the 6 $f_i^{(b)}$ values that act on the centroid, $(\mathbf{X}_\alpha^{(p)}, Z_\alpha^{(p)})$, of the α^{th} element on the surface of the protofilament.

With translational and rotational velocities (u_x, u_y, u_z) and $(\omega_x, \omega_y, \omega_z)$ obtained through Eq. 13, the location of the center of the protofilament, at $\mathbf{x} = (X_0, Y_0, Z_0)$ and the center's Euler parameters are determined, via the procedure outlined in Tjavaras et al. (41), as

$$\frac{d}{dt} \begin{bmatrix} X_0 \\ Y_0 \\ Z_0 \end{bmatrix} = \begin{bmatrix} u_x \\ u_y \\ u_z \end{bmatrix} = \mathbf{C}^{-1} \cdot \begin{bmatrix} u_x \\ u_y \\ u_z \end{bmatrix},$$

$$\frac{d}{dt} \begin{bmatrix} \beta_0 \\ \beta_1 \\ \beta_2 \\ \beta_3 \end{bmatrix} = \frac{1}{2} \begin{bmatrix} \beta_0 & -\beta_1 & -\beta_2 & -\beta_3 \\ \beta_1 & \beta_0 & -\beta_3 & \beta_2 \\ \beta_2 & \beta_3 & \beta_0 & -\beta_1 \\ \beta_3 & -\beta_2 & \beta_1 & \beta_0 \end{bmatrix} \cdot \begin{bmatrix} 0 \\ \omega_x \\ \omega_y \\ \omega_z \end{bmatrix}. \quad (17)$$

Equation 17 is integrated via central differences.

Stretching force within the Sp

The strain-stress relation of the Sp is modeled using the WLC model. This model depicts a polymer such as a Sp as a

continuous elastic cable possessing constant bending stiffness characterized by a persistence length, a measure of the average curvature along the contour (31). By considering thermal equilibrium, the WLC model provides a closed-form description of the stretch-tension relation of the polymer that is easy to implement. However, it ignores the transient behavior of the polymer and the randomness of the tension. To include the randomness, we use a modified form of the WLC and express the tension-stretching relation as

$$f^{(s)} = \frac{k_B T}{p} \left[\frac{1}{4(1 - \ell/L_c)^2} - \frac{1}{4} + \frac{\ell}{L_c} \right] + \Delta f^{(s)}, \quad (18)$$

where the first term in the right-hand side is the original WLC expression. The value ℓ is the distance between the two ends of Sp, p the persistence length, and L_c the contour length. To date there is no widely accepted value of p . Its reported value varies from 0.8 nm (32) and 2.5 nm (42) to 10 nm (43) and depends on the folded versus unfolded state of the Sp. In the following computation, we choose $p = 8$ nm, which yields a prediction of the shear modulus consistent with existing studies. We take $L_c = 144$ nm. The thermal fluctuation term, $\Delta f^{(s)}$, is prescribed to be a Gaussian random variable with zero mean and a standard deviation, δ_f , which is preevaluated using a cable-dynamics polymer model, which is essentially a WLC model in the time domain. Through numerical simulations we find that this standard deviation is proportional to $\Delta t^{-1/2}$, and is insensitive to the changes in either ℓ or L_c . Summarizing the results, we choose $\delta_f \Delta t^{1/2} = 9 \times 10^{-17} \text{ N s}^{1/2}$ (see Appendix for a more detailed description).

In their recent model studies, Discher et al. (19) and Li et al. (20) have modeled steric repulsion between the Sps of a JC by adding a term to the free energy of the form C/A , where A represents the area associated with the JC. C is a constant evaluated by setting the net pressure within the skeleton (assumed not attached to a bilayer) to zero once the JC attains a prescribed rest area; this also sets the length of the Sp at which steric repulsion, so modeled, balances the tension within the Sp. The steric contribution contributes to the area modulus but not to the area preserving shear modulus. Since in the present study the SCs are fixed to the bilayer, the bilayer supports pretension in the Sp segments and our skeleton does not collapse. Future modeling will include a detailed account of steric interaction such as we have presented here for steric interactions between the protofilament and the Sp with the bilayer itself. This will be necessary since we allow for SC mobility. For now we note that the effect of inter-Sp repulsion as modeled in the literature (18–20) is essentially on the computation of the area modulus, κ_s , of the skeleton itself (i.e., without the dominant effect of the bilayer on area stiffness)—and which can be analytically shown to amount to $\kappa_s \approx 2\mu$ (μ being the predicted skeleton shear modulus when computed at the rest area of the JC). As noted, the Sp WLC model used here does not include the extension softening that

would come about due to either intramolecular transitions such as Sp domain unfolding, or interprotein events such as spectrin head-to-head disassociation. Models for such events are further considered in Conclusions and Discussion.

Elastic energy of the lipid bilayer/skeleton membrane

The elastic energy of the system contains three parts, the stretching energy stored in the bilayer owing to pretension, the elastic energy of the bilayer due to elevation by bending and via pretension (the combination of these is called $\Phi^{(b)}$), and the strain energy in the Sp, called $\Phi^{(s)}$. In this study, the process that induces pretension is not considered—so that for the total elastic energy, we only consider $\Phi^{(b)}$ and $\Phi^{(s)}$. The elastic energy due to bending and pretension is

$$\Phi^{(b)} = \iint_{L \times L} d\mathbf{X} \left\{ \frac{\kappa}{2} [\nabla^2 h(\mathbf{X}, t)]^2 + \frac{\sigma}{2} |\nabla h(\mathbf{x}, t)|^2 \right\}. \quad (19)$$

The strain energy stored within a single Sp is obtained by integrating the incremental work of extension (i.e., the mean tension as given in Eq. 18 times $d\ell$) to give

$$\phi^{(s)} = \frac{k_B T}{4p} \left(\frac{3\ell^2 - 2\ell^3/L_c}{L_c - \ell} \right). \quad (20)$$

The total energy stored in the six Sp is called $\Phi^{(s)}$.

NUMERICAL RESULTS

With the hybrid numerical algorithm described in the previous section, we conducted numerical simulations to illustrate the static and dynamic response of the JC coupled to the lipid bilayer. In our numerical simulations the size of the computational domain was chosen to be $L = 400$ nm. 64×64 Fourier modes were used to represent deformation of the bilayer. For numerical stability in the time integration, a small time step of 0.1 ns was employed.

Quasi-static response

We first analyze the quasi-static response of the coupled JC-bilayer system without considering thermal fluctuations. Starting from an arbitrary initial state, the motion of this system was simulated until a steady state was reached. The steady values of the orientation angles of the protofilament, including the yaw angle and the pitch angle as defined in the inset in Fig. 4 and the deformation of the bilayer, as well as the strain energy $\Phi^{(b)}$ and $\Phi^{(s)}$, are summarized below. Moreover, to examine the dependence of the quasi-static response of the JC with respect to the lipid bilayer pretension (σ), we applied the point-attachment junction and simulated the yaw and pitch angles of the protofilament in the natural state as functions of σ . It was found that the pretension had no significant effect upon the yaw angle of the protofilament. What

was found (data not shown) was that at values of $\sigma > 10^{-3}$ Nm the pitch angle decreased from 7° to $\sim 5^\circ$. This suggests a stiffening of the bilayer at sufficiently high levels of σ . Bilayer stiffening is manifested in a reduction in the ratio between energy associated with bending (the first term in Eq. 19) and that associated with the pretension (the second term). At low levels of σ , the energy due to bending is much larger than that due to the pretension, yet when $\sigma \gtrsim 4 \times 10^{-4}$ Nm $^{-1}$ the two contributions are equal and reverse their order of magnitude at larger pretension. In the following examples we have chosen $\sigma = 10^{-4}$ Nm $^{-1}$, where the effects of bending and pretension are comparable.

As shown in Figs. 2 and 3 *a*, we assume that in its natural state the six SCs in a basic unit form a hexagon. A general in-plane stretch of the JC, corresponding to a topology-conserving redeployment of the SCs within the lipid bilayer, can be represented as a stretching along an arbitrary axis within the *X*-*Y* plane (denoted as axis 1) by a ratio λ_1 , plus a stretching by a ratio λ_2 along a second axis which also lies within the *X*-*Y* plane and is normal to axis 1. The angle between axis 1 and the *X* axis, measured counterclockwise, is defined as the deformation angle τ . An equibiaxial deformation refers to an in-plane stretching in which $\lambda_1 = \lambda_2$. As illustrated in Fig. 3 *b*, an equibiaxial deformation results in a similar hexagon enlarged by a factor of λ^2 . Therefore, the equibiaxial deformation is τ -independent, and is related to an area change of the membrane skeleton. During the deformation, the lipids may flow into or out of the changing area spanned by the SCs, because the SCs may be dragged through the bilayer with little resistance, as noted above. Although the natural viscosity that this fluidic motion of lipid molecules contributes is not considered in this study, one can imagine that it will have significant effects on the dynamics of the coupled system. Fig. 4 shows the equilibrium orientation of the protofilament during an equibiaxial deformation from

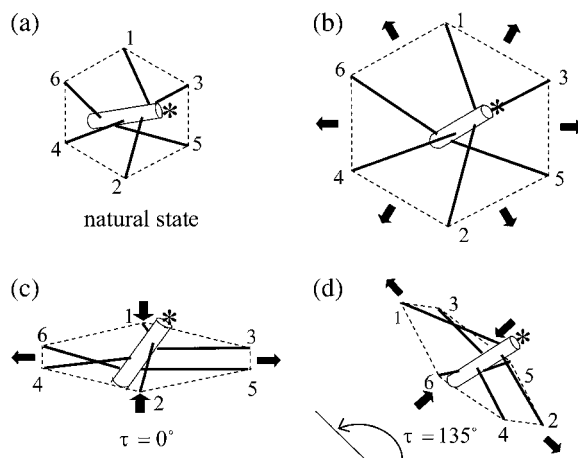


FIGURE 3 Schematic illustrating the natural state (*a*), a state corresponding to equibiaxial extension (*b*), and anisotropic deformations (*c* and *d*) as defined by the deformation angle τ . The pointed end of the protofilament is marked with an asterisk. Arrows point to the direction of deformation.

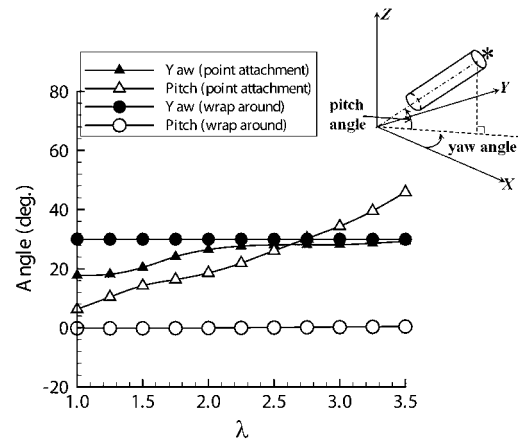


FIGURE 4 Dependence of the attitude of the protofilament on the extension ratio (λ) in equibiaxial deformation. The inset defines the yaw and pitch angles. The pointed end of the protofilament is marked with an asterisk.

$\lambda = 1$ to $\lambda = 3.5$. The two Sp-protofilament junctions predict dramatically different behaviors of the protofilament. With the point-attachment junction, the yaw angle varies from 18° at the natural state to $\sim 30^\circ$ at $\lambda = 3.5$. The change in pitch angle is more profound, varying from 6° at $\lambda = 1$ to 46° at $\lambda = 3.5$, indicating a bow-up tendency with increasing dilation. With the wrap-around junction, on the other hand, the orientation of the protofilament is much less sensitive to the deformation. Within the whole range that we consider, the yaw angle remains at 30° , and the pitch angle is close to 0° , so that the axis of the protofilament is almost parallel to the bilayer.

An anisotropic deformation is an in-plane stretching of the JC in which the area of the hexagon is preserved, i.e., $\lambda_1 \lambda_2 = 1$. As shown in Fig. 3, *c* and *d*, an anisotropic deformation depends on the deformation angle, τ , as well as the stretching ratio. In this case, as the area is conserved, we imagine that the lipid bilayer undergoes a viscous shear. This adds a viscous strain rate to the elastic shear deformability to be described. Fig. 5, *a* and *b*, show the orientation of the protofilament at $\tau = 0^\circ$ and 135° and $\lambda = 1$ to 3.5 obtained by using the point-attachment junction. The most noteworthy phenomenon is the bifurcation in the orientation of the protofilament. At both deformation angles, two equilibrium states are identified for each extension ratio λ provided that it is sufficiently large. For example, we consider the case with deformation angle $\tau = 0^\circ$. The threshold λ for bifurcation is ~ 1.05 . For any λ larger than that value, two sets of yaw/pitch angles (each representing an equilibrium state) are shown. One of these states occurs at yaw angle $\sim 70^\circ$, the other at $\sim -70^\circ$. The two states have similar pitch angles and are almost identical in terms of the total elastic energy, $\Phi^{(s)} + \Phi^{(b)}$. This bifurcation can be explained by the close symmetry of the JC configuration with respect to the *X* axis, or an axis that is 60° , 90° , or 120° , from the *X* axis. The symmetry is not exact because the Sps have different lengths during deformation.

With the point-attachment junction, the model also predicts dramatic variation of the yaw angle with respect to the extension ratio. For instance, at $\tau = 0^\circ$ near $\lambda = 1.05$ the yaw angle quickly increases from 18° to 70° . This behavior, together with the bifurcation, indicates that the JC configuration described by using the point-attachment junction is quite unstable during anisotropic deformations. In contrast, using the wrap-around junction the model predicts a much more stable JC. As shown in Fig. 5, *c* and *d*, in most cases the attitude varies slowly with the extension ratio. Among all the cases we studied, the only bifurcation occurs at $\tau = 135^\circ$, and at a relatively high extension ratio $\lambda = 2$. The pitch angle remains small.

The predictions using the wrap-around junction (Figs. 4 and 5) are more consistent with experimental observations. For example, according to Picart et al. (24,25), during deformation the protofilaments remain tangent to the bilayer. The point-attachment junction, on the other hand, predicts large pitch angles in equibiaxial deformations (Fig. 4). Clearly, additional attention needs to be paid to the molecular structure of such junctions as the results show that the two, albeit extreme cases in terms of induced axial moment, impart quite different behavior to the JC.

To illustrate the effect of the lipid bilayer on the equilibrium state of the JC, simulations were also performed using a decoupled system without the bilayer. With the wrap-around junctions, the results are close to the predictions via the coupled JC-bilayer simulation mentioned above. In contrast, with the point-attachment junction, the results are different with

and without the lipid bilayer. Without the lipid bilayer (and the repulsive force imposed) the attitude of the protofilament is not sensitive to deformations. In both equibiaxial and anisotropic deformations, yaw angles remain at $\sim 30^\circ$ and pitch angles at $\sim 70^\circ$.

The disturbance on the bilayer exerted by the JC is highly localized and concentrated in the vicinities of the SCs and the contacting point between the protofilament and the lipid bilayer. The magnitude of this disturbance is significantly affected by the pitch angle of the protofilament. With the point-attachment junction, and, for example, for an equibiaxial extension of $\lambda = 3.5$, the pitch angle of the protofilament is $\sim 46^\circ$, leading to a maximum elevation of 3 nm (occurring near the SCs connected with Sp_1 and Sp_2). In contrast, the wrap-around junction leads to a pitch angle close to 0° , suggesting that the protofilament is almost parallel to the lipid bilayer. The corresponding maximum elevation is only 1 nm (occurring right beneath the protofilament). In general, the pitch angles predicted by using the wrap-around junction are much smaller than those predicted by using the point-attachment junction (Fig. 4). These results indicate that by using the wrap-around junction, the disturbance by the protofilament on the bilayer is significantly reduced. This is clearly demonstrated in Fig. 6, which shows that during equibiaxial deformation, a JC with the wrap-around junction generates a much smaller elastic energy inside the bilayer than a JC with the point-attachment junction.

The elastic response of the hybrid protein skeleton/lipid bilayer membrane is represented by its elastic moduli, which

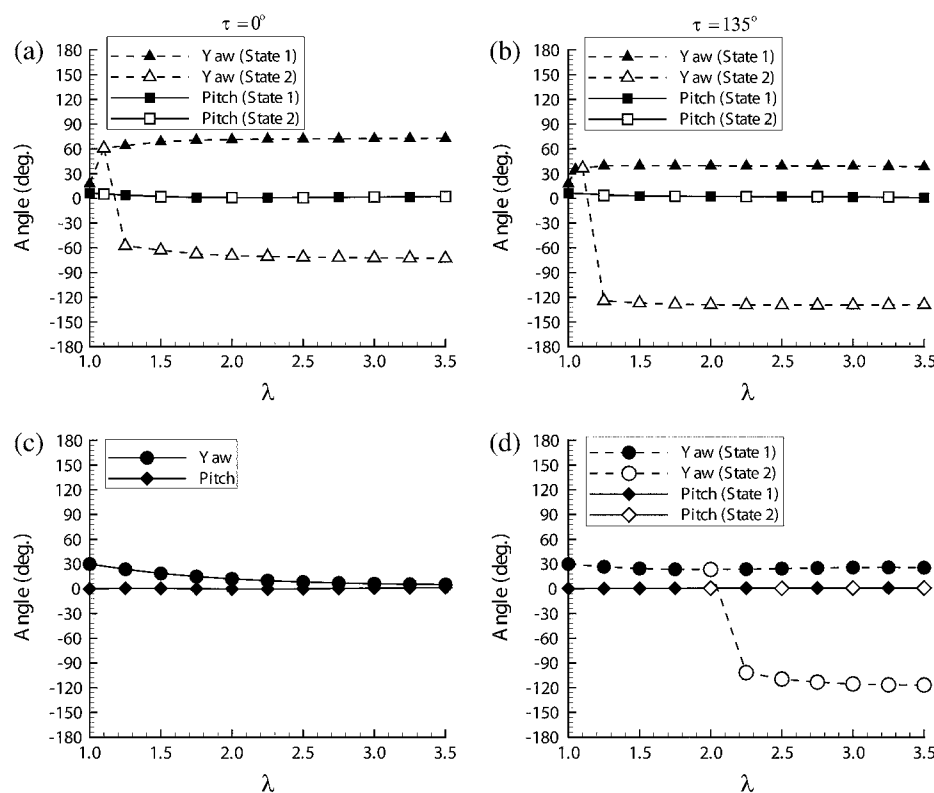


FIGURE 5 Dependence of pitch and yaw angles on stretch during anisotropic deformation with (a) $\tau = 0^\circ$ and using the point-attachment model, (b) $\tau = 135^\circ$ and using the point-attachment model, (c) $\tau = 0^\circ$ and using the wrap-around model, and (d) $\tau = 135^\circ$ and using the wrap-around model.

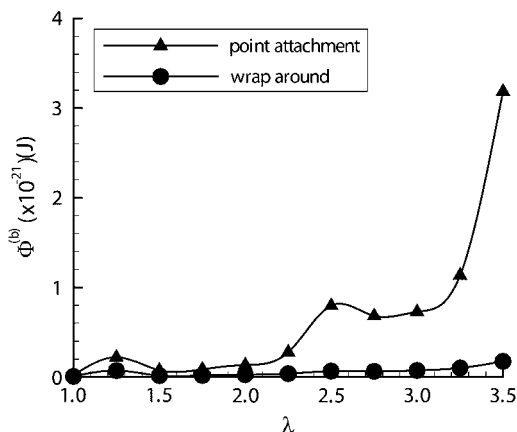


FIGURE 6 The elastic energy in the lipid bilayer as a function of the extension ratio (λ) in equibiaxial deformation.

are obtained herein via quasi-static deformations. For in-plane deformations, the relevant elastic moduli are the area and shear moduli. Since the lipid bilayer possesses very limited compressibility, it dominates the area modulus of the composite structure. The protein skeleton, on the other hand, contributes significantly to the shear modulus of the structure and thus is our focus here. Following Evans and Skalak (6), we calculate the shear modulus of the JC undergoing finite deformations using a method based on the strain energy, $\Phi^{(s)}$, stored in the Sp. In this approach, an arbitrary deformation is characterized by two independent deformation parameters $\alpha = \lambda_1\lambda_2 - 1$ and $\beta = (\lambda_1^2 + \lambda_2^2)/(2\lambda_1\lambda_2) - 1$. Here α represents area change, and β a change of aspect ratio or eccentricity. The shear modulus, μ , is then given as

$$\mu = \frac{1}{A_0} \left. \frac{\partial \Phi^{(s)}}{\partial \beta} \right|_{\alpha=0}, \quad (21)$$

where A_0 is the reference area, which is the projected area occupied by the JC (the hexagon) in its natural state. For the configuration defined in Fig. 2, $A_0 = 2.34 \times 10^{-15} \text{ m}^2$. Constraining $\alpha = 0$ corresponds to an area-conserving anisotropic deformation.

With the hybrid model, we find that the shear modulus is heavily influenced by the persistence length p of the Sp. Indeed, with the configuration of the JC prescribed and the extension ratio fixed, we are able to show that μ is roughly proportional to $1/p$ as would be expected by the $1/p$ scaling within the WLC model. Consequently, accurate determination of the persistence length p is critical to the evaluation of shear modulus via our model. Owing to the inconclusiveness concerning the exact value of p , in Fig. 7 we plot μ normalized by $k_B T/pL_c$. The point-attachment junction and the wrap-around junction provide similar predictions for μ , while the variation over different deformation angle τ is $\sim 20\%$ with the maximum value occurring near $\tau = 90^\circ$. We note that by using $p = 8 \text{ nm}$, our model of the single JC unit predicts that at a small deformation, i.e., $\lambda = 1.25$, $\mu = 7 \times 10^{-6} \text{ N/m}$. This is close to predictions obtained in other reports (2,4–6,

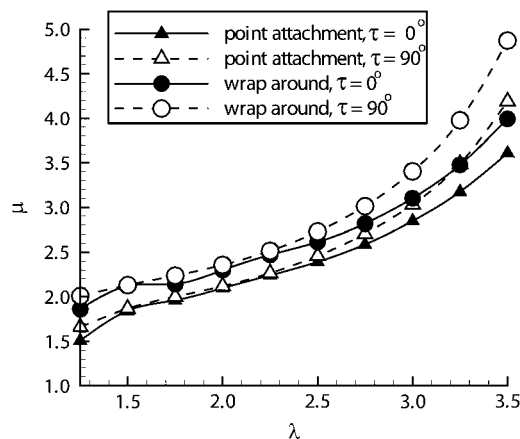


FIGURE 7 Shear modulus of a single JC unit coupled with the lipid bilayer normalized by $k_B T/pL_c$ obtained with the point-attachment junction and wrap-around junction.

18–20,42,43). Fig. 7 indicates strain stiffening of the network consistent with other modeling results (e.g., (20)), whereas evidence for increasing network compliance with extension has been obtained by measuring the fluctuations of fluorescent beads attached to the network during micropipette aspirations (33). As noted, this may be attributed to effects such as domain unfolding within the Sp or possibly interprotein disassociation.

Effect of thermal fluctuations

We further studied the response of the hybrid JC/lipid bilayer subject to thermal fluctuations. As illustrated in Fig. 8,

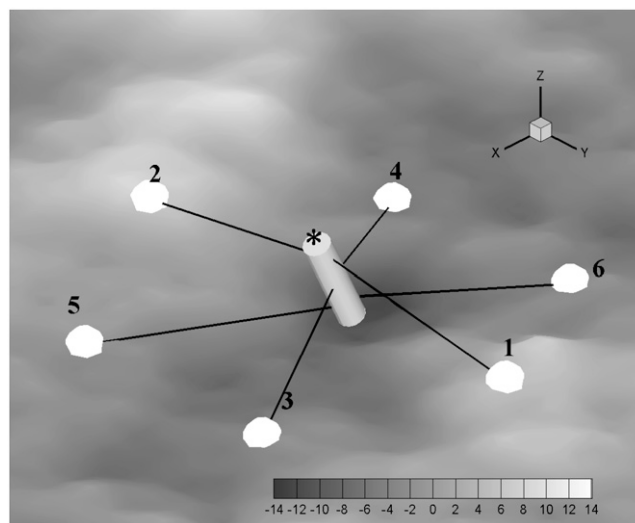


FIGURE 8 Snapshot of an equibiaxially extended JC ($\lambda = 2.5$) during thermal fluctuation obtained with the point-attachment junction. The protofilament is shown as a cylinder, the SCs are shown as spheres, and the elevation of lipid bilayer is shown by the contour (bright areas represent high elevation and dark areas are low elevation, with the contours in nanometers). The pointed end of the protofilament is marked with an asterisk.

corresponding to the Brownian motion, a stochastic wavelike motion is seen to occur within the lipid bilayer. In addition, the JC itself is subject to a random vibration. The mean values and standard deviations of the attitude of the actin protofilament in an equibiaxial deformation obtained with both the point-attachment and the wrap-around junctions are extracted from the simulations. What is found is that the mean values of both the yaw and the pitch angles are close to the quasi-static predictions. With the point-attachment junction, the deviation of the yaw angle decreases from 64° at $\tau = 1$ to 44° at $\tau = 3.5$. Similarly, with the wrap-around junctions, this deviation decreases from 49° to 21° . Such oscillation reduction is due to an increased tethering force from the Sp. The deviation of the pitch angle, caused primarily by the thermal fluctuation of the bilayer, remains at $\sim 25^\circ$ and is not sensitive to τ .

Corresponding to the bifurcation discussed before, a mode-switching phenomenon is observed in anisotropic deformations. A mode-switching event is shown in Fig. 9, with $\tau = 0^\circ$ and $\lambda = 3.5$, and using the point-attachment junction. In this simulation, the yaw angle jumps from $\sim -70^\circ$ (corresponding to state 2 in Fig. 5 *a*) to 70° (state 1) within a short time of $\sim 5 \mu\text{s}$. The transition process is often accompanied by an abrupt increase of pitch angle up to 80° ,

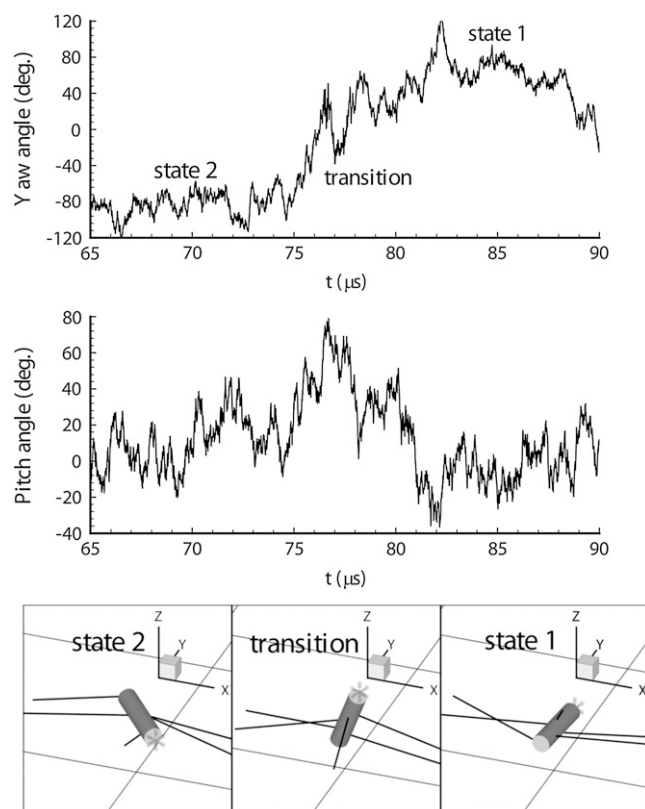


FIGURE 9 A mode-switching event during thermal oscillation of the JC in anisotropic deformation with $\lambda = 3.5$ and deformation angle $\tau = 0^\circ$. The result was obtained with the point-attachment junction. The pointed end of the protofilament is marked with an asterisk.

indicating a bow-up motion (see Fig. 9). This motion is expected to affect the structural stability of the network and increase the disturbance on the bilayer. The actual occurrence of mode switching, however, is expected to be affected by more subtle molecular structures of the membrane not yet included in the model, e.g., the secondary linkages between the protofilament and the lipid bilayer through protein 4.1 and glycophorin C.

CONCLUSIONS AND DISCUSSION

The mechanical properties of the membrane are important for erythrocyte deformation. The actin/spectrin-based network has been studied for more than three decades, and the wealth of information on the system continues to motivate modeling efforts. When modeled at the molecular level the investigation may shed new light into how elements in the network may respond to the deformation and what may be the physiological consequences. Among the key insights provided by this model is that how spectrin associates with actin may influence the dynamics of a protofilament in response to deformation.

Here we present the first computational model that incorporates the static and the dynamic responses of a single JC coupled to a lipid bilayer subjected to external loads. These studies are perhaps the first to examine the hydrodynamic aspect of a model with certain degrees of molecular detail. The coupling simulated in this report is through the primary linkage at the SCs. New features considered in this model include two types of junctions between the actin protofilament and the Sp (i.e., point-attachment and wrap-around). The conjectured molecular detail of the wrap-around model is shown in Fig. 10. In both equibiaxial (area-changing) and anisotropic (area-conserving) deformations, the structural responses with the wrap-around junction are much more stable than those with the point-attachment junction. In contrast to the point-attachment junction, in which the orientation of the protofilament is much affected by the amount of deformation and the presence of the lipid bilayer, the wrap-around junction diminishes the sensitivity to deformations and the JC-bilayer interactions. The wrap-around junction also leads to a reduced pitch angle for the protofilament, consistent with experiments (24,25), and the motion of the protofilament exerts much less disturbance on the lipid bilayer. In addition, the wrap-around junction suppresses the occurrence of bifurcations in anisotropic deformations, which is the existence of more than one equilibrium state at a certain extension ratio and deformation angle. The bifurcation originates from the symmetric distribution of the SCs (forming a regular hexagon), the three-dimensional geometry of the protofilament, the protofilament-bilayer interaction, and the manner of Sp-protofilament connection, which allow the existence of multiple minima in terms of the total strain energy stored in the Sp. In the dynamic response of the system with thermal fluctuations, a bifurcation may cause mode switching, in which the system

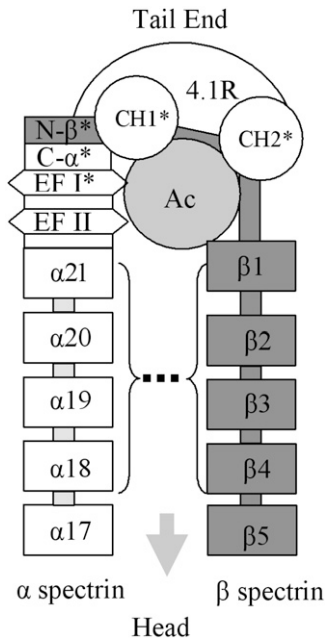


FIGURE 10 A proposed Sp wrap around the actin protofilament annotated with known spectrin domains. The tail end of Sp begins with the nonhomologous domains in the C-terminus of α -spectrin (C- α) and N-terminus of β -spectrin (N- β) (26,52). Nonhomologous domains are involved in the interchain binding at the tail end (29), but not in the dimer nucleation (27). The dimer nucleation sites spanning homologous domains of β 1–4 and α 18–21 are proximal (27). The actin-binding domains (ABD) are on β -spectrin, comprised of two Calponin Homology (CH) subdomains (53). There are two EF hand domains at the C-terminal α -spectrin (54). Some of Cys residues (*) at the tail end may be active, capable of forming disulfide bonds (27). Protein 4.1R stabilizes the binding between β -spectrin and F-actin, with a split β -spectrin binding site binding to CH1 and CH2, and an actin binding site positioned in between (28,45,55).

switches from one equilibrium state to another within a short time interval. A mode-switching event is often accompanied by a bow-up/bow-down motion of the protofilament, i.e., a sudden increase/decrease of the pitch angle. This type of motion imposes a large transient load on the lipid bilayer, which may affect the structural stability of the membrane and its physiological performance. These simulations suggest the importance of three-dimensional molecular junctions and the lipid bilayer/protein network coupling on cell membrane mechanics.

This hybrid model forms a framework upon which a sequence of more sophisticated models, which will include additional molecular detail as well as other factors such as the viscoelasticity of the lipid bilayer and that of the Sp (see e.g., (44)), will be developed. The resulting multiple-scale model may provide a method of understanding the exact role each molecular component may play in terms of the overall mechanical performance of the membrane. A near-term extension of our model will include the secondary linkage between the protein network and the lipid bilayer at JC involving actin, protein 4.1, and the transmembrane glycoprotein C (45,46). The mechanical function of these secondary link-

ages and their physiological importance to the membrane will be simulated with sufficient three-dimensional molecular detail to describe the interactions among them. Our preliminary simulations show that these secondary linkages may diminish the thermal fluctuation of the protofilament.

Future studies will involve simulations of multiple units of JCs (see Fig. 2 *b*) attached to a dynamic bilayer as described herein. The goal will be to model the effects of SC mobility, the connectivity between JC and SC, and molecular detail of the linkages between the protein network and the lipid bilayer on overall membrane mechanical response. Based on published values for the short range diffusion coefficient of band 3 (22), we have estimated the mobility for the SC. Band 3 is mobile within the plane of the lipid bilayer and this mobility would give rise to a time-dependent viscoelastic response of the network. The short range diffusion coefficient, D , of band 3 in the lipid bilayer at 37°C is $0.53 \mu\text{m}^2 \text{s}^{-1}$ (22), which corresponds to a mobility (via Brownian dynamics) of $D/k_B T = 1.28 \times 10^8 \text{m(Ns)}^{-1}$. Typical levels of tension inside an Sp during network deformation, based on our previous model (17) and the simulations reported on here, is estimated in the range of 2–10 pN. Under this forcing, the time for the SC to drift a distance comparable to the size of a JC ($\sim 70 \text{ nm}$) is $\sim 55\text{--}270 \mu\text{s}$. It is thus expected that the SC will be seen to be dragged through the lipid bilayer in a timescale associated with cell deformations, e.g., $\sim 0.1 \text{ s}$ in micropipette aspirations. In the future analysis of ensembles of JCs we will allow SC mobility within the bilayer, and we note that this imparts an entirely natural viscosity to the protein network/lipid bilayer response as yet unaccounted for. On the other hand, during the deformation of the entire cell the lipid bilayer must follow the global deformation and thus undergo shear in parallel with the skeleton. Later in describing the computed shear modulus we will add a viscous term accounting for this viscous contribution to the shear resistance. Multiple JC units, connected through periodic boundary conditions, will allow for the free motion of SCs—i.e., via a force-mobility relation as prescribed with the mobility described above. In this way lipid molecules will be seen to flow in and out of the areas occupied by individual JCs. Particular studies will include topological changes that are characteristic of certain diseases, where mutations have been identified in membrane skeletal components, such as those in hereditary spherocytosis, ovalocytosis, or elliptocytosis. Simulations involving multiple JCs, as depicted in Fig. 2 *b*, will include descriptions of Sp disassociation from actin or from the head-to-head dimer connections, or Sp unfolding/folding, as influenced by Sp tension (32,47). The formalism for such descriptions can follow an analysis based on thermally activated kinetics whereby one expresses rate of disassociation, or transitions, in the form

$$k_{\alpha \rightarrow \beta} = \nu_m k_{\alpha \rightarrow \beta}^0 \exp\left(\frac{f^{(s)} \Delta x_{\alpha \rightarrow \beta}^*}{k_B T}\right), \quad k_{\alpha \rightarrow \beta}^0 = \exp\left(\frac{\Delta G}{k_B T}\right), \quad (22)$$

where ν_m is a frequency term that is related to the attempt frequency of the transition and thus is dependent on the molecular (mechanical) configuration; α, β represent two states, e.g., folded or unfolded Sp states; $f^{(s)}$ is the tension inside; $\Delta G_{\alpha \rightarrow \beta}$ is the activation energy at $f^{(s)} = 0$ for the transition $\alpha \rightarrow \beta$; and $\Delta x_{\alpha \rightarrow \beta}^*$ is the transition length (akin to an activation volume in solid state kinetics). Lee and Discher (33) have, in fact, provided a start in this direction and have suggested a possible force-displacement model for Sp undergoing unfolding/refolding transitions. Models for Sps of this type are readily included as input to our simulations and will be explored in future work. It remains for future study to explore the possibility of extension-driven unstiffening via simulations using Sp force-extension constitutive laws that account for unfolding \rightarrow refolding transitions.

Our hybrid model is capable of predicting the dynamics of individual components of the erythrocyte membrane, and has demonstrated good agreement with other models (e.g., (18–20)) and experimental results (e.g., (24,25)). It also could be applied in the interpretation of experiments involving localized behavior of the membrane, e.g., the thermal fluctuation of membrane attached beads or quantum-dots. By simulating the thermal oscillation of a bead attached to the protofilament using our model incorporating unfolding of Sp repeats in large stretching, our preliminary results suggest an increase in bead fluctuation accompanying large shear deformation, a trend observed in experiments (33). This increase in fluctuation may be attributed to both the unstiffening effect due to unfolding of repeats, the onset of mode switching, or other mechanisms. Further investigations to quantitatively correlate our numerical predictions with experimental measurements are underway and will be reported in a forthcoming report. There are recently developed technologies that make measuring the three-dimensional orientation of biomolecules possible. For example, single-molecule fluorescence polarization microscopy has been used to determine the three-dimensional orientation of a single F-actin in vitro (48); and single-pair fluorescence resonance energy transfer using a wide-field total-internal-reflection fluorescence microscopy has been used to image single molecules in living cells, providing a quantitative measuring of inter- and intramolecular distances and angles (49). These innovative techniques may allow the attitude changes of a protofilament to be recorded during membrane deformation, thus providing a way to test our model.

APPENDIX: TENSION-STRAIN RELATION OF THE SP

The dynamic response of a flexible biopolymer such as an Sp is typically modeled as Gaussian polymer (GP), free-jointed chain (FJC), or wormlike chain (WLC). In the GP model the polymer is composed of a series of particles joined by springs, while the FJC model assumes that the biopolymer consists of bonds of fixed length that can point in any direction independently of each other. The WLC model is a continuous model that overcomes the sharp bends occurring in the GP model or the FJC model. In WLC, the biopolymer is described as an elastic continuous curve at thermal equilib-

rium with uniform elastic constants. A persistence length characterizes its bending energy. The WLC model is also easy to apply since it provides a closed-form description of the stretch-tension relation of the polymer. In its original form, however, WLC only provides a description of the average behavior of a large group of polymers over a long time. The transient behavior of the polymer and the randomness of the tension are ignored.

To calculate the transient behavior of a polymer using the WLC description, a direct numerical simulation cable-dynamics model has been developed (50). Essentially a WLC model in time domain, this model depicts the biopolymer as an elastic cable that can be bent and twisted with finite curvature everywhere. The internal tension, bending moment, and twisting moment are all continuous functions along the molecule. Unlike the WLC model, however, in the cable-dynamics model the mathematical formulation governing the biopolymer's dynamic behavior is obtained according to first principles—that is, conservation of mass, momentum, and energy. The motion of the polymer at any instant is determined by the balance among the internal elastic forces and moments as described by the cable-dynamics formulation (41), the fluid force obtained from Eqs. 14 and 15 (with the diameter of the Sp chosen to be 2 nm), and thermal fluctuations evaluated through Brownian dynamics. Numerical algorithms are developed to perform time-domain simulations. On the one hand, this time-domain WLC model enables direct simulation of the transient behavior of an individual polymer. On the other hand, this model is much more computationally involved than WLC since it requires high spatial resolutions that can only be achieved by employing a large number of grids along the contour of the polymer (and, correspondingly, an extremely small time step for numerical stability).

To predict the time-dependent behavior of Sp without solving the expensive cable-dynamics equations, we develop a modified WLC depiction of the tension-stretching relation by expressing the tension inside the spectrin as the linear superposition of the original WLC expression and a thermal fluctuation term $\Delta f^{(s)}$. The thermal fluctuation is prescribed to be a Gaussian random variable with zero mean and a deviation δf , which is preevaluated using the cable-dynamics model. To achieve this, we fix the distance l between the two ends of the Sp, and record the instantaneous tension force acting on these ends toward each other. From the time history of this recorded force, the standard deviation is calculated as a function of the time step Δt , the contour length L_c , and the extension l . By doing this, we find that this deviation is proportional to $\Delta t^{-1/2}$, and it is insensitive to the changes in either l or L_c . Summarizing the results, we choose $\delta f \Delta t^{1/2} = 9 \times 10^{-17} \text{ N s}^{1/2}$.

We thank the Department of Bioengineering for providing access to its new 210-node Dell PowerEdge Linux Supercomputer to perform the simulations.

REFERENCES

1. Lipowsky, H. H., C. B. McKay, and J. Seki. 1989. Trans time distributions of blood flow in the microcirculation. In *Microvascular Mechanics: Hemodynamics of Systems and Pulmonary Microcirculation*. Springer-Verlag, New York.
2. Waugh, R. E., and P. Agre. 1988. Reductions of erythrocyte-membrane viscoelastic coefficients reflect spectrin deficiencies in hereditary spherocytosis. *J. Clin. Invest.* 81:133–141.
3. Liu, S. C., J. Palek, S. J. Yi, P. E. Nichols, L. H. Derick, S. S. Chiou, D. Amato, J. D. Corbett, M. R. Cho, and D. E. Golan. 1995. Molecular basis of altered red blood cell membrane properties in Southeast Asian ovalocytosis: role of the mutant band 3 protein in band 3 oligomerization and retention by the membrane skeleton. *Blood*. 86:349–358.
4. Mohandas, N., and E. Evans. 1994. Mechanical properties of the red cell membrane in relation to molecular structure and genetic defects. *Annu. Rev. Biophys. Biomol. Struct.* 23:787–818.
5. Discher, D. E., N. Mohandas, and E. A. Evans. 1994. Molecular maps of red cell deformation: hidden elasticity and in situ connectivity. *Science*. 266:1032–1035.

6. Evans, E., and R. Skalak. 1980. *Mechanics and Thermodynamics of Biomembranes*. CRC Press, Boca Raton, FL.
7. Sung, K. L., and S. Chien. 1992. Influence of temperature on rheology of human erythrocytes. *Chin. J. Physiol.* 35:81–94.
8. Byers, T. J., and D. Branton. 1985. Visualization of the protein associations in the RBC membrane skeleton. *Proc. Natl. Acad. Sci. USA*. 82:6153–6157.
9. Shen, B. W., R. Josephs, and T. L. Steck. 1986. Ultrastructure of the intact skeleton of the human RBC membrane. *J. Cell Biol.* 102:997–1006.
10. Liu, S. C., L. H. Derick, and J. Palek. 1987. Visualization of the hexagonal lattice in the RBC membrane skeleton. *J. Cell Biol.* 104:527–536.
11. Sung, L. A., and C. Vera. 2003. Protofilament and hexagon: a three-dimensional mechanical model for the junctional complex in the erythrocyte membrane skeleton. *Ann. Biomed. Eng.* 31:1314–1326.
12. Cohen, C. M., J. M. Tyler, and D. Branton. 1980. Spectrin-actin associations studied by electron microscopy of shadowed preparations. *Cell*. 21:875–883.
13. Bennett, V., and P. J. Stenbuck. 1979. The membrane attachment protein for spectrin is associated with band 3 in human RBC membranes. *Nature*. 280:468–473.
14. Risinger, M. A., C. Korsgren, and C. M. Cohen. 1996. Role of *n*-myristylation in targeting of band 4.2 (pallidin) in nonerythroid cells. *Exp. Cell Res.* 229:421–431.
15. Reid, M. E., Y. Takakuwa, J. Conboy, G. Tchernia, and N. Mohandas. 1990. Glycophorin C content of human erythrocyte membrane is regulated by protein 4.1. *Blood*. 75:2229–2234.
16. Bennett, V., and A. J. Baines. 2001. Spectrin and ankyrin-based pathways: metazoan inventions for integrating cells into tissues. *Phys. Rev.* 81:1353–1392.
17. Vera, C., R. Skelton, F. Bossens, and L. A. Sung. 2005. 3-D nanomechanics of an erythrocyte junctional complex in equibiaxial and anisotropic deformations. *Ann. Biomed. Eng.* 33:1387–1404.
18. Boey, S. K., D. H. Boal, and D. E. Discher. 1998. Simulations of the erythrocyte cytoskeleton at large deformation. I. Microscopic models. *Biophys. J.* 75:1573–1583.
19. Discher, D. E., D. H. Boal, and S. K. Boey. 1998. Simulations of the erythrocyte cytoskeleton at large deformation. II. Micropipette aspiration. *Biophys. J.* 75:1584–1597.
20. Li, J., M. Dao, C. T. Lim, and S. Suresh. 2005. Spectrin-level modeling of the cytoskeleton and optical tweezers stretching of the erythrocyte. *Biophys. J.* 88:3707–3719.
21. Hansen, J. C., R. Skalak, S. Chien, and A. Hoger. 1997. Influence of network topology on the elasticity of the red blood cell membrane skeleton. *Biophys. J.* 72:2369–2381.
22. Lin, L. C., and F. L. Brown. 2005. Dynamic simulations of membranes with cytoskeletal interactions. *Phys. Rev. E Stat. Nonlin. Soft Matter Phys.* 72:011910.
23. Granek, R. 1997. From semi-flexible polymers to membranes: anomalous diffusion and reptation. *J. Phys. III*. 7:1761–1788.
24. Picart, C., and D. E. Discher. 1999. Actin protofilament orientation at the erythrocyte membrane. *Biophys. J.* 77:865–878.
25. Picart, C., P. Dalhaimer, and D. E. Discher. 2000. Actin protofilament orientation in deformation of the erythrocyte membrane skeleton. *Biophys. J.* 79:2987–3000.
26. Winkelman, J. C., J. G. Chang, W. T. Tse, A. L. Scarpa, V. T. Marchesi, and B. G. Forget. 1990. Full-length sequence of the cDNA for human erythroid beta-spectrin. *J. Biol. Chem.* 265:11827–11832.
27. Harper, S. L., G. E. Begg, and D. W. Speicher. 2001. Role of terminal nonhomologous domains in initiation of human red cell spectrin dimerization. *Biochemistry*. 40:9935–9943.
28. An, X., G. Debnath, X. Guo, S. Liu, S. E. Lux, A. Baines, W. Gratzer, and N. Mohandas. 2005. Identification and functional characterization of protein 4.1r and actin-binding sites in erythrocyte beta spectrin: regulation of the interactions by phosphatidylinositol-4,5-bisphosphate. *Biochemistry*. 44:10681–10688.
29. Viel, A., and D. Branton. 1994. Interchain binding at the tail end of the *Drosophila* spectrin molecule. *Proc. Natl. Acad. Sci. USA*. 91:10839–10843.
30. Law, R., S. Harper, D. W. Speicher, and D. E. Discher. 2004. Influence of lateral association on forced unfolding of antiparallel spectrin heterodimers. *J. Biol. Chem.* 279:16410–16416.
31. Marko, J. F., and E. D. Siggia. 1995. Stretching DNA. *Macromolecules*. 28:8759–8770.
32. Rief, M., J. Pascual, M. Saraste, and H. E. Gaub. 1999. Single molecule force spectroscopy of spectrin repeats: low unfolding forces in helix bundles. *J. Mol. Biol.* 286:553–561.
33. Lee, J. C., and D. E. Discher. 2001. Deformation-enhanced fluctuations in the red cell skeleton with theoretical relations to elasticity, connectivity, and spectrin unfolding. *Biophys. J.* 81:3178–3192.
34. Kas, J., H. Strey, J. X. Tang, D. Finger, R. Ezzell, E. Sackmann, and P. A. Janmey. 1996. F-actin, a model polymer for semiflexible chains in dilute, semidilute, and liquid crystalline solutions. *Biophys. J.* 70:609–625.
35. Whittaker, E. T. 1989. *A Treatise on the Analytical Dynamics of Particles and Rigid Bodies*. Cambridge University Press, Cambridge, UK.
36. Junkins, J. L., and J. D. Turner. 1986. *Optimal Spacecraft Rotational Maneuvers*. Elsevier Science Publishers, Amsterdam, The Netherlands.
37. Podgornik, R., and V. A. Parsegian. 1992. Thermal-mechanical fluctuations of fluid membranes in confined geometries: the case of soft confinement. *Langmuir*. 8:557–562.
38. Doi, M., and S. F. Edwards. 1986. *The Theory of Polymer Dynamics*. Oxford University Press, Oxford, UK.
39. Lighthill, J. 1976. Flagellar hydrodynamics: The John Von Neumann Lecture. *SIAM Rev.* 18:161–230.
40. Lamb, H. 1932. *Hydrodynamics*, 6th Ed. Dover Publication, Mineola, NY.
41. Tjavaras, A. A., Q. Zhu, Y. Liu, M. S. Triantafyllou, and D. K. P. Yue. 1998. The mechanics of highly-extensible cables. *J. Sound Vibr.* 213:709–737.
42. Lenormand, G., S. Henon, A. Richert, J. Simeon, and F. Gallet. 2003. Elasticity of the human red blood cell skeleton. *Biorheology*. 40:247–251.
43. Scoboda, K., C. F. Schmidt, D. Branton, and S. M. Block. 1992. Conformation and elasticity of the isolated red blood cell membrane skeleton. *Biophys. J.* 63:784–793.
44. Levine, A. J., and F. C. MacKintosh. 2002. Dynamics of viscoelastic membranes. *Phys. Rev. E Stat. Nonlin. Soft Matter Phys.* 66:061606.
45. Discher, D. E., R. Winardi, P. O. Schischmanoff, M. Parra, J. G. Conboy, and N. Mohandas. 1995. Mechanochemistry of protein 4.1's spectrin-actin-binding domain: ternary complex interactions, membrane binding, network integration, structural strengthening. *J. Cell Biol.* 130:897–907.
46. Reid, M. E., Y. Takakuwa, J. Conboy, G. Tchernia, and N. Mohandas. 1990. Glycophorin C content of human erythrocyte membrane is regulated by protein 4.1. *Blood*. 75:2229–2234.
47. Rief, M., M. Gautel, F. Oesterhelt, J. M. Fernandez, and H. E. Gaub. 1997. Reversible unfolding of individual titin immunoglobulin domains by AFM. *Science*. 276:1109–1112.
48. Forkey, J. N., M. E. Quinlan, and Y. E. Goldman. 2005. Measurement of single macromolecule orientation by total internal reflection fluorescence polarization microscopy. *Biophys. J.* 89:1261–1271.
49. Webb, S. E., S. R. Needham, S. K. Roberts, and M. L. Martin-Fernandez. 2006. Multidimensional single-molecule imaging in live cells using total internal reflection fluorescence microscopy. *Opt. Lett.* 31:2157–2159.
50. Zhu, Q., J. Zeng, M. S. Triantafyllou, and D. K. P. Yue. 2006. Direct numerical simulation of single-molecule DNA by cable dynamics. *J. MEMS*. 15:1078–1087.

51. Alberts, B., A. Johnson, J. Lewis, M. Raff, K. Roberts, and P. Walter. 2002. *Molecular Biology of the Cell*, 4th Ed. Garland Science, Taylor & Francis Group, New York.
52. Sahr, K. E., P. Laurila, L. Kotula, A. L. Scarpa, E. Coupal, T. L. Leto, A. J. Linnenbach, J. C. Winkelmann, D. W. Speicher, and V. T. Marchesi. 1990. The complete cDNA and polypeptide sequences of human erythroid alpha-spectrin. *J. Biol. Chem.* 265:4434–4443.
53. Bramham, J., J. L. Hodgkinson, B. O. Smith, D. Uhrin, P. N. Barlow, and S. J. Winder. 2002. Solution structure of the calponin CH domain and fitting to the 3D-helical reconstruction of F-actin:calponin. *Structure*. 10:249–258.
54. Lundberg, S., J. Bjork, L. Lofvenberg, and L. Backman. 1995. Cloning, expression and characterization of two putative calcium-binding sites in human non-erythroid alpha-spectrin. *Eur. J. Biochem.* 230:658–665.
55. Horne, W. C., S. C. Huang, P. S. Becker, T. K. Tang, and E. J. Benz, Jr. 1993. Tissue-specific alternative splicing of protein 4.1 inserts an exon necessary for formation of the ternary complex with erythrocyte spectrin and F-actin. *Blood*. 82:2558–2563.